

A controlled destruction and progressive collapse of 2D reinforced concrete frames

Mourid El Houcine, Mamouri Said, Adnan Ibrahimbegović

▶ **To cite this version:**

Mourid El Houcine, Mamouri Said, Adnan Ibrahimbegović. A controlled destruction and progressive collapse of 2D reinforced concrete frames. Coupled systems mechanics, 2018, 7, pp.111 - 139. 10.12989/csm.2018.7.2.111 . hal-01996745

HAL Id: hal-01996745
https://hal.utc.fr/hal-01996745

Submitted on 13 Feb 2019

HAL is a multi-disciplinary open access archive for the deposit and dissemination of scientific research documents, whether they are published or not. The documents may come from teaching and research institutions in France or abroad, or from public or private research centers.

L'archive ouverte pluridisciplinaire **HAL**, est destinée au dépôt et à la diffusion de documents scientifiques de niveau recherche, publiés ou non, émanant des établissements d'enseignement et de recherche français ou étrangers, des laboratoires publics ou privés.

Coupled Systems Mechanics, *Vol. 7, No. 2 (2018) 111-139*
DOI: https://doi.org/10.12989/csm.2018.7.2.111

A controlled destruction and progressive collapse of 2D reinforced concrete frames

Mourid El houcine[1], Mamouri Said[*1] and Ibrahimbegovic Adnan[2]

[1]*Université de Tahri Mohamed-Bechar, Algeria*
[2]*Université de Technologie Compiègne/Sorbonne universités, France*

(Received June 6, 2017, Revised July 8, 2017, Accepted July 9, 2017)

Abstract. A successful methodology for modelling controlled destruction and progressive collapse of 2D reinforced concrete frames is presented in this paper. The strategy is subdivided into several aspects including the failure mechanism creation, and dynamic motion in failure represented with multibody system (MBS) simulation that are used to jointly capture controlled demolition. First phase employs linear elasto-plastic analysis with isotropic hardening along with softening plastic hinge concept to investigate the complete failure of structure, leading to creation of final failure mechanism that behaves like MBS. Second phase deals with simulation and control of the progressive collapse of the structure up to total demolition, using the nonlinear dynamic analysis, with conserving/decaying energy scheme which is performed on MBS. The contact between structure and ground is also considered in simulation of collapse process. The efficiency of the proposed methodology is proved with several numerical examples including six story reinforced concrete frame structures.

Keywords: complete collapse; multibody system; plastic joint; geometrically exact beam; energy conserving/decaying scheme; contact

1. Introduction

This work deals with aging reinforced concrete building presenting the high risk of failure due to natural disaster or at the end of their lifespan. The research has been carried out on controlled progressive collapse of those structures. Where full understanding of complete failure mechanism is needed in densely populated urban areas in order to avoid the damage to adjacent structure. Due to the complexity of this kind of problems, only a few works provide a safe and economically reasonable method for simulating the structure demolition, with a special attention required to the progressive collapse process.

Some research uses explosive technics for building demolition. Such a strategy is based on explosives placed at well-determined zones in the building (Michaloudis *et al.* 2010) and Michaloudis *et al.* 2011). Other works are based on blasting strategy eliminating some vertical supports in the structure and exploiting the force of gravity (Hartmann *et al.* 2008).

*Corresponding author, Professor, E-mail: said.mamouri@gmail.com

Copyright © 2018 Techno-Press, Ltd.
http://www.techno-press.org/?journal=csm&subpage=8 ISSN: 2234-2184 (Print), 2234-2192 (Online)

the work in (Rodolfo and Humberto 2017) presents finite element methodology that can be used to simulate progressive collapse of planar frame. Such strategy is based on the dynamical detachment of lose finite elements assembled by Lagrange multipliers. Therefore, such technics can only be used for describing the quasi-brittle behavior of the analyzed structure. More general, ductile behavior was considered in (Humberto and Rodrigo 2014) where the elasto-plastic law and nonlinear behavior of semi-rigid connections are adopted for planar frames.

Many recent papers give a particular attention for numerical modelling of discontinuities (Nanakorn 2004, Juarez and Ayala 2012), and softening plastic hinges in finite element beams and frames (Armero and Ehrlich 2006, Wu 2013). A multi scale model for reinforced concrete frames is given in (Pham *et al.* 2013), introducing embedded strain discontinuity in fiber and a systematic procedure for estimating frame model parameters. A combined stress resultant beam model and a shell model is presented in (Dujc *et al.* 2010), for computing the complete failure of metal frames. In the same manner, a Weak coupling of shell and beam computational models for failure analysis of steel frames is studied in (Piculin and Brank 2015). An Euler-Bernoulli stress resultant beam model for failure analysis of planar RC beams and frames, considering only the bending failure mechanism, is described in (Jukic *et al.* 2013). The same authors present in (Jukic *et al.* 2014) a multilayer beam finite element formulation for failure analysis of planar reinforced concrete frames that combines damage, plasticity and embedded discontinuity. The works in (Bui *et al.* 2014, Imamovic *et al.* 2017) present both bending and shear failure mechanism, using an enriched Timoshenko beam for failure analysis.

In present work, we develop a new methodology that can be used for modelling of controlled progressive collapse of planar reinforced concrete structures. Our strategy can be summarized as follow:

1. The creation of mechanism by applying a geometrically linear analysis based on elasto-plastic law with bilinear isotropic hardening. The plastic hinges are governed by a softening rigid-plastic law. We suppose that, up to the plastic hinges formation and mechanism creation, the response of structure is indeed geometrically linear, and that there is no need for considering large rotations and displacements.
2. Nonlinear dynamic multibody system simulation based on total Lagrangian formulation and Reissner's beam kinematics, where the failing parts of the structure behave like rigid bodies during the progressive collapse process. An efficient conserving/decaying energy scheme developed by Mamouri *et al.* (2016a) is used for solving governing dynamic equations.
3. Simulation of contact between structure and ground is adopted to describe the final phases in demolition of structure and its behavior after total collapse.

Our strategy for progressive collapse is subdivided into several phases of the problem analysis, based on failure mechanism creation, mechanism simulation as multibody system and controlled demolition as final phase. The proposed strategy present advantages such as:

(i) The ability to describe the response of reinforced concrete structure from the cracking and reinforcement yielding until total failure, post-peak behaviour, and failure mechanism creation.

(ii) The formation of plastic hinges is done automatically during the analysis at the critical zones, providing an efficient modelling in failure mechanism creation.

(iii) The use of an efficient conserving/decaying time integration scheme with constant mass matrix that provides a desirable numerical dissipation in higher modes and reliable presentation of full collapse.

(iv) The ability of modelling the contact problem between the structure and the ground in simplified way by using an efficient algorithm based on penalty method, to provide the risk

estimate of damage to adjacent structure.

The outline of this paper is as follows. In the next section we present the theoretical formulation of geometrically exact beam model for concrete failure analysis. In subsequent two sections we provide, respectively the constitutive relations in hardening and softening plastic hinge in bending. In Section 2, we present the model of mechanism created using multibody system approach based on master-slave technics and the conserving/decaying time stepping schemes. In the subsequent section we provide the description of the model for contact between the structure and the ground. In the last section we show the results for several numerical simulations illustrating the proposed methodology. The last section gives several concluding remarks.

2. Beam model for failure analysis

The localized material failure in critical zones is the reason behind the collapse of the most reinforced concrete frame structures (Dujc *et al.* 2010). In opposite to the classical limit load analysis, which is not able to describe the post-peak behavior, the softening plastic hinge is characterized by increase of displacement at decrease of loading (Jukic *et al.* 2013, Bui*et al.* 2014, Imamovic *et al.* 2017, Ngo *et al.* 2014). The model ingredients are as follow: First, a 2D Timoshenko finite element beam with standard kinematics is presented. The bending is governed by an elasto-plastic law with bi-linear isotropic hardening. Second, in order to model the softening plastic hinge, the embedded discontinuity has to be taken in account when describing the beam kinematics (see Jukic *et al.* 2013, Bui *et al.* 2014, Imamovic *et al.* 2017, Ngo *et al.* 2014). For our case, we deal with displacement field enhanced with jump discontinuity in rotation. The response at plastic hinge is described by softening rigid-plastic law.

2.1 Standard kinematics

We consider a (curved) Timoshenko beam of length L and cross section *A*. The initial configuration of the beam is specified by the position vector $\boldsymbol{\varphi}_0$ of a point on the neutral axis$s \in [0\,, L]$ and the unit vector$\boldsymbol{t}_1^0$ normal of the beam cross section (see Ibrahimbegovic and Mamouri 1999)

$$\boldsymbol{t}_1^0 = \boldsymbol{\varphi}_0' \tag{1}$$

where $(\bullet)' = \frac{d}{ds}(\bullet)$ denotes the partial derivative with respect to the s-coordinate.

According to Timoshenko/Reissner's hypothesis, the plane section remains plane after deformation but not necessarily perpendicular to the neutral axis of the beam (see Ibrahimbegovic and Frey 1993a). The deformed configuration can thus be defined as

$$\boldsymbol{\phi}(s,t,\zeta) = \boldsymbol{\varphi}(s,t) + \zeta \boldsymbol{t}_2(s,t) \tag{2}$$

where $\boldsymbol{\varphi}(s) = \begin{pmatrix} x+u \\ y+v \end{pmatrix}$ is the position of a point on the neutral axis; whereas $\boldsymbol{t}_2$ is the unit vector attached to the beam cross section.

In accordance with the basic kinematic hypothesis, the unit vectors $\boldsymbol{t}_1$ and $\boldsymbol{t}_2$ are obtained by rotation from their initial positions $\boldsymbol{t}_1^0$ and $\boldsymbol{t}_2^0$. Thus, we define a two-dimensional rotation matrix as

$$\boldsymbol{t}_1 = \boldsymbol{\Lambda}\boldsymbol{t}_1^0,\ \ \boldsymbol{t}_2 = \boldsymbol{\Lambda}\boldsymbol{t}_2^0,\ \ \boldsymbol{\Lambda} = \begin{bmatrix} cos\,\psi & -sin\,\psi \\ sin\,\psi & cos\,\psi \end{bmatrix} \tag{3}$$

where ψ is the rotation angle around$\boldsymbol{t}_3$.

The generalized strain measure (Mamouri *et al.* 2014) can be written as

$$\begin{cases} \boldsymbol{\varepsilon} = \boldsymbol{\varphi}' - \boldsymbol{t}_1 \\ k = \psi' \boldsymbol{t}_3 \end{cases} \tag{4}$$

Where $\boldsymbol{\varepsilon}$ contain axial and shear strain and k is the corresponding bending strain.

When considering the small displacement and small rotation theory (Ibrahimbegovic and Frey 1993a), we can write a simplified linearized form of the governing kinematics equations as

$$\cos\psi \approx 1 \quad and \quad \sin\psi \approx \psi \ , \qquad \boldsymbol{t_1} = \begin{pmatrix} 1 \\ \psi \end{pmatrix} \tag{5}$$

We consider 2D finite element beam with 2node and lengthl^e.

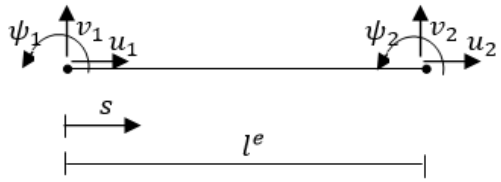


Fig. 1 two nodes beam finite element with 3 degree of freedom per node

The displacement field corresponding to the chosen finite element beam model is written as

$$\begin{cases} u(s) = N_1(s)u_1 + N_2(s)u_2 = \boldsymbol{N}\boldsymbol{u} \\ v(s) = N_1(s)v_1 + N_2(s)v_2 = \boldsymbol{N}\boldsymbol{v} \\ \psi(s) = N_1(s)\psi_1 + N_2(s)\psi_2 = \boldsymbol{N}\boldsymbol{\psi} \end{cases} \tag{6}$$

where $\boldsymbol{u}\ and\ \boldsymbol{v}$ respectively are the axial and transverse components of the nodal displacement vector $\boldsymbol{\varphi}$. $\boldsymbol{\psi}$ is the nodal rotation vector.

$\boldsymbol{N} = \left\{N_1(s) = 1 - \frac{s}{l^e},\ N_2(s) = \frac{s}{l^e}\right\}$ Are the shape functions.

The discretized form of the beam element deformations can be written as

$$\begin{cases} \varepsilon(s) = \boldsymbol{B}\boldsymbol{u} \\ \gamma(s) = \boldsymbol{B}\boldsymbol{v} - \boldsymbol{N}\,\boldsymbol{\psi} \\ \kappa(s) = \boldsymbol{B}\boldsymbol{\psi} \end{cases} \tag{7}$$

Where $\boldsymbol{B} = \left\{-\frac{1}{l^e};\ \frac{1}{l^e}\right\}$

2.2 Constitutive relations

We suppose that the response in axial direction is linear elastic leading to axial force; $N =$

$EA\bar{\varepsilon}$, where E is elastic modulus, A is cross section area and $\bar{\varepsilon}$ is axial strain. However, the bending is described by elasto-plasticity with bilinear isotropic hardening which fits well with behavior of RC structures (Ibrahimbegovic and Frey 1993b). (See Fig. 2). The behavior is linear elastic up to M_C where the first crack in concrete appears. After that, the behavior is elastoplastic linear with hardening response up to M_y when yielding of the reinforcement causes change in hardening modulus.

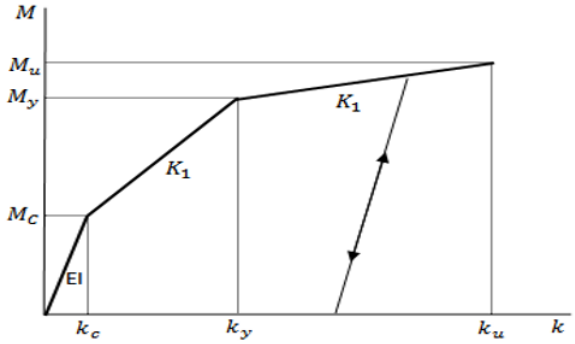


Fig. 2 Moment-curvature relation for bending stress resultant model

The curvature is decomposed into elastic and plastic part.

$\kappa = \bar{\kappa}^e + \bar{\kappa}^p$(8)

The yield criterion is described by the yield function$\bar{\phi}$

$$\bar{\phi}(M, \bar{q}) = |M| - (M_c - \bar{q}) \tag{9}$$

$$M = \mathrm{EI}(\bar{\kappa} - \bar{\kappa}^p) \tag{10}$$

where I is the inertia moment and $\bar{q}$is the stress like bending hardening variable that depends linearly on the strain like bending hardening variable $\bar{\xi}$ (Jukic*et al.* 2013).

$$\bar{q} = \begin{cases} -K_{h1}\bar{\xi} \\ -(M_y - M_c)\left(1 - \dfrac{K_{h2}}{K_{h1}}\right) - K_{h2}\bar{\xi} \end{cases} \tag{11}$$

Where K_{h1} and K_{h2} are hardening moduli.

The evolution equations for plastic strain and hardening variable are

$$\dot{\bar{\kappa}}^p = \dot{\bar{\gamma}} sign(M);\ \dot{\bar{\xi}} = \dot{\bar{\gamma}} \tag{12}$$

The loading\unloading condition and the consistency conditions are

$$\dot{\bar{\gamma}} \geq 0\ ;\ \ \bar{\phi} \leq 0\ \ ;\ \dot{\bar{\gamma}}\bar{\phi} = 0\ ;\ \dot{\bar{\gamma}}\dot{\bar{\phi}} = 0 \tag{13}$$

2.3 Enhanced kinematics with rotation discontinuity

In order to represent the effect of softening plastic hinge, a jump in rotation α is defined at

point s_d on the neutral axis. The expression of rotation after considering the jump α is given by (Bui *et al.* 2014)

$$\psi(S) = \bar{\psi}(S) + \alpha H_\Gamma \tag{14}$$

where $\bar{\psi}(S)$ is the regular part rotation, and $H_\Gamma \alpha$ is the singular part.
with

$$H_\Gamma = \begin{cases} 0 & if\ s < s_d \\ 1 & if\ s \geq s_d \end{cases} \tag{15}$$

The expression of total rotation can be written as

$$\psi(S) = \tilde{\psi}(S) + \alpha\big(H_\Gamma - \Omega(S)\big) \tag{16}$$

where

$$\tilde{\psi}(S) = \bar{\psi}(S) + \alpha\Omega(S) \tag{17}$$

and

$$\Omega(S) = \begin{cases} 0 & if\ s = 0 \\ 1 & if\ s = L \end{cases} \tag{18}$$

With this particular form, the contribution of discontinuity is canceled on the element nodes and does not further propagates into the domain. (for more detail for the choice of $\Omega(S)$ see (Bui *et al.* 2014)

The curvature $k(s)$of the element can be also decomposed into a regular part and a singular part

$$\kappa(s) = \bar{\kappa}(s) + \alpha\delta_{x_d}(s) \tag{19}$$

where $\bar{\kappa}(s)$ denotes the regular part of the curvature. α with the Dirac delta function δ_{x_d} denotes the singular part of rotation of hinge at point s_d (Jukic*et al.* 2013).

The displacement field corresponding to the finite element beam with 2 nodes including rotation discontinuity is written as

$$\begin{cases} u(s) = N_1(s)u_1 + N_2(s)u_2 \\ v(s) = N_1(s)v_1 + N_2(s)v_2 \\ \psi(s) = N_1(s)\psi_1 + N_2(s)\psi_2 + \big(H_\Gamma - N_2(s)\big)\alpha \end{cases} \tag{20}$$

where α is the jump in rotation.

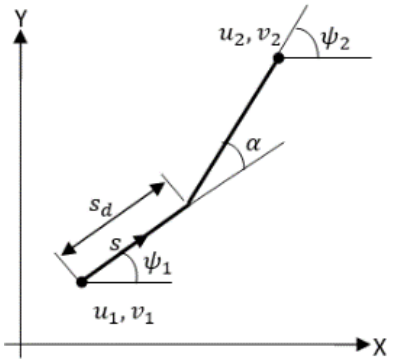


Fig. 3 The jump rotation α within an element

The discretized form of the beam element deformations including the jump in rotation can be written as

$$\begin{cases} \varepsilon(x) = \boldsymbol{Bu} \\ \gamma(x) = \boldsymbol{Bv} - \boldsymbol{N\psi} \\ \kappa(x) = \boldsymbol{B\psi} + G\alpha \end{cases} \tag{21}$$

where $G = \bar{G} + \bar{\bar{G}} = -\frac{1}{l^e} + \delta_{x_d}$

The generalized deformations ordered in a matrix can be expressed as

$$\boldsymbol{\varepsilon}(s) = \boldsymbol{Bd} + \boldsymbol{G\alpha} \tag{22}$$

with

$$\boldsymbol{B} = (\boldsymbol{B_1}, \boldsymbol{B_2});\ \boldsymbol{B_i} = \begin{bmatrix} \frac{dN_i}{ds} & 0 & 0 \\ 0 & \frac{dN_i}{ds} & -N_i \\ 0 & 0 & \frac{dN_i}{ds} \end{bmatrix} \tag{23}$$

and

$$\boldsymbol{G} = \bar{\boldsymbol{G}} + \bar{\bar{\boldsymbol{G}}} = \begin{bmatrix} 0 \\ 0 \\ -\frac{1}{l^e} \end{bmatrix} + \begin{bmatrix} 0 \\ 0 \\ 1 \end{bmatrix} \delta_{x_d} \tag{24}$$

The general vector of nodal displacement is defined as

$$\boldsymbol{d} = \langle u_1, v_1, \psi_1, u_2, v_2, \psi_2 \rangle^T \tag{25}$$

The weak form of the equilibration equation can be written for two levels: global that concerns all elements and local that concerns particular elements with activated hinges (see Bui *et al.* 2014). A typical element contribution at these two levels can be written as

$$\begin{cases} \int_0^{l^e} \boldsymbol{d}^{*T} \boldsymbol{B}^T \boldsymbol{\sigma} ds - \int_0^{l^e} \boldsymbol{d}^{*T} \boldsymbol{N}^T \boldsymbol{f} ds - \boldsymbol{d}^{*T} \boldsymbol{F} = 0 \\ \int_0^{l^e} \alpha^* \boldsymbol{G^T} \boldsymbol{\sigma} ds = 0 \qquad\qquad \forall e \in [1, N_{el}^{\alpha}] \end{cases} \tag{26}$$

By using the finite element assembly procedure (e.g., see Zienkiewicz and Taylor 2005), we obtain the set of global and local equations

$$\begin{cases} A_{e=1}^{Nel} \left[\boldsymbol{f}^{int(e)} - \boldsymbol{f}^{ext(e)} \right] = 0\,, \qquad \forall e \in [1\,, N_{el}] \\ h^e = \int_0^{l^e} \bar{G}\, M ds + M_{s=s_d} = 0\,, \forall e \in [1, N_{el}^{\alpha}] \end{cases} \tag{27}$$

Here $\boldsymbol{f}_{int}^{(e)}$ is the internal force vector

$$\boldsymbol{f}_{int}^{(e)} = \int_0^{l^e} \boldsymbol{B}^T \boldsymbol{\sigma} ds \tag{28}$$

and $\boldsymbol{f}_{ext}^{(e)}$ is the external force vector

$$\boldsymbol{f}_{ext}^{(e)} = \int_0^{l^e} \boldsymbol{N}^T \boldsymbol{f} ds + \boldsymbol{F} \tag{29}$$

The first equation in (27) enforces the equilibrium at all the nodes in the mesh, and the second requires weak equilibrium between the moment at discontinuity and moment in the bulk for each element in the mesh with activated plastic hinge.

By using consistent linearization (Ibrahimbegovic 2009); we obtain the equilibrium equations (27) written in the incremental form

$$\begin{cases} A_{e=1}^{Nel}\left[\boldsymbol{K}^{fd}\Delta\boldsymbol{d} + \boldsymbol{K}^{f\alpha}\Delta\alpha - \boldsymbol{f}^{ext(e)}\right] = 0 \\ \boldsymbol{K}^{hd}\boldsymbol{\Delta d} + K^{h\alpha}\Delta\alpha = 0 \end{cases} \tag{30}$$

where

$\boldsymbol{K}^{fd} = \int_0^{l^e} \boldsymbol{B}^T \boldsymbol{C}\, \boldsymbol{B} ds$; $\quad \boldsymbol{K}^{f\alpha} = \int_0^{l^e} \boldsymbol{B}^T \boldsymbol{C}\, \bar{\boldsymbol{G}} ds$

$\boldsymbol{K}^{hd} = \int_0^{l^e} \bar{\boldsymbol{G}}^T \boldsymbol{C}\, \boldsymbol{B} ds$; $\quad K^{h\boldsymbol{\alpha}} = \int_0^{l^e} \bar{G} C\, \bar{G} ds + k_s$

By static condensation at the element level, the Eq. (30) turns into

$$A_{e=1}^{Nel}\left[\widehat{\boldsymbol{K}}^e \Delta\boldsymbol{d} - \boldsymbol{f}^{ext(e)}\right] = 0 \tag{31}$$

With

$$\widehat{\boldsymbol{K}}^e = \boldsymbol{K}^{fd} - \boldsymbol{K}^{f\alpha}(K^{h\boldsymbol{\alpha}})^{-\mathbf{1}}\boldsymbol{K}^{hd} \tag{32}$$

The solution of this equation will give the corresponding displacement increment and new displacement.

2.4 Softening plastic hinge in bending

When the ultimate moment M_u is reached at s_d (the most critical cross section), the rotation discontinuity is activated as is described before, and the softening plastic hinge forms at the same location. The moment in the hinge is related to the jump in rotation by rigid softening plastic response. Fig. 4 shows that the moment in plastic hinge decrease linearly with increase of jump rotation (see Jukic *et al.* 2013).

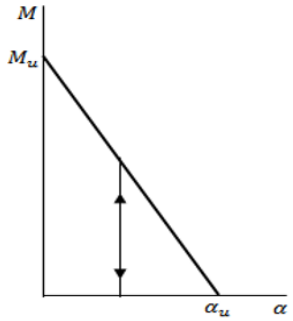


Fig. 4 Moment-jump relation for softening

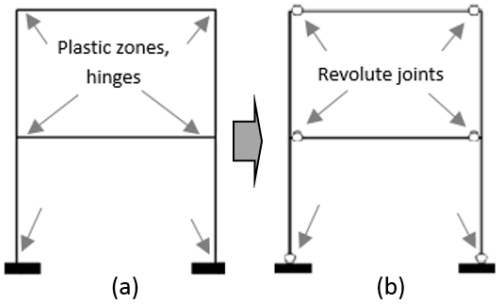


Fig. 5 Replacing softening plastic hinges with revolute joints

We note that during the softening process, the moment in plastic hinge remains in weak equilibrium with the moment in the bulk of finite element.

The plastic hinge forms at the most critical cross section, generally, at integration point where we first reach the ultimate moment. After activation of the plastic hinge, all components of the curvature expressions are non-zero. The plastification process of the bulk material stops and plastic curvature will not be changing anymore (Jukic *et al.* 2013). The curvature decomposes into elastic, plastic and singular part

$$\kappa = \bar{\kappa}^e + \bar{\kappa}^p + \bar{\bar{\kappa}} \tag{33}$$

with $\bar{\kappa}^p$ that remains frozen subsequently.

The failure yield function $\bar{\bar{\phi}}$ can be written as

$$\bar{\bar{\phi}}(t, \bar{\bar{q}}) = |t| - (M_u - \bar{\bar{q}}) \tag{34}$$

$$t = -\int_0^{l^e} \bar{G} M dx \tag{35}$$

where $\bar{\bar{q}}$ represents bending moment like softening variable, which grows linearly with internal strain-like bending softening variable $\bar{\bar{\xi}}$ up to M_u when carrying capacity drops to zero (Jukic *et al.* 2013)

$$\bar{\bar{q}} = min\left\{-K_{s\bar{\bar{\xi}}} \; ; \; M_u\right\}; \; K_s < 0 \tag{36}$$

The evolution equations for softening variable, the loading/unloading conditions and the consistency conditions are

$$\dot{\alpha} = \dot{\bar{\bar{\gamma}}} sign(M); \; \dot{\bar{\bar{\xi}}} = \dot{\bar{\bar{\gamma}}} \tag{37}$$

$$\dot{\bar{\bar{\gamma}}} \geq 0 \; ; \quad \bar{\bar{\phi}} \leq 0 \; ; \dot{\bar{\bar{\gamma}}} \bar{\bar{\phi}} = 0 \; ; \; \dot{\bar{\bar{\gamma}}} \dot{\bar{\bar{\phi}}} = 0 \tag{38}$$

3. Dynamic nonlinear analysis of multibody system

The application of the theoretical aspects and computations described in previous part provides

a structure completely or partially failed. After formation of most plastic hinges, the structure obtained a new equilibrium state, with redistribution of the stress resultants and moments, giving a mechanism like multibody system. For well representing the behavior of mechanism, we replace the plastic hinges with the revolute joints which allow a free components rotation in the plane (see Fig. 5).

3.1 Joints constraint and relative motion

The joint is defined when two beam elements are not rigidly attached to each other. In particular, the revolute joint allows a free rotation of the two adjacent elements around a given axis. With the chosen master-slave approach, one of connected nodes in joint is called a master and the other node is called slave (see Ibrahimbegovic and Mamouri 2000).

The motions of the master and the slave nodes in 2D are specified by their position vectors and rotation matrices

$$\boldsymbol{\varphi}_t^m, \boldsymbol{\Lambda}_t^m = [\boldsymbol{t}_1^m, \boldsymbol{t}_2^m];\ \boldsymbol{\varphi}_t^s, \boldsymbol{\Lambda}_t^s = [\boldsymbol{t}_1^s, \boldsymbol{t}_2^s] \tag{39}$$

The master and slave nodes share the same coordinates, which allows us to write

$$\boldsymbol{\varphi}_t^s - \boldsymbol{\varphi}_t^m = 0 \tag{40}$$

Such constraint can be handled by using the Lagrange multiplier procedure, which requires adding to the equilibrium equations, a supplementary condition according to

$$\lambda_\varphi(\boldsymbol{\varphi}_t^s - \boldsymbol{\varphi}_t^m) = 0 \tag{41}$$

where λ_φ is the Lagrange multiplier. Such an approach leads to considerable increase in total number of global unknowns, in addition to the unknown motion components for both master and slave nodes (for more detail see Ibrahimbegovic and Mamouri 2000). In order to avoid this constraint, we propose an alternative approach, which consist to impose the master slave joint constraint kinematic; by considering a relative motion. In the case of revolute joint, the coordinates of slave node are the same as those of the master node. The slave node rotation matrix can be obtained as the multiplication of the master node rotation matrix and relative rotation matrix. The slave node rotation matrix can be defined as

$$\boldsymbol{\Lambda}_t^s = \boldsymbol{\Lambda}_t^m \boldsymbol{\Lambda}_t^r \tag{42}$$

where $\boldsymbol{\Lambda}_t^r$ is the relative rotation matrix. In 2D, the rotation of slave node can be expressed as sum of master node rotation and a given relative rotationψ^r

$$\psi^s = \psi^m + \psi^r \tag{43}$$

This approach can be used in our work to represent MBS which is employed here for modelling the controlled progressive collapse. Such process requires the ability of describing large rotations and displacements. Thus, a nonlinear dynamic analysis must be applied using geometrically nonlinear Reissner's beam as the proper generalization of the Timoshenko beam from the first phase of the analysis. In the following section, we present nonlinear kinematic beam and time integration scheme.

3.2 Non-linear Reissner's beam kinematic with master-slave constraint

In this section, we describe the equations governing the motion of 2D beam presented in section 1 considering large rotations and displacements (Mamouri *et al.* 2014, Mamouri *et al.* 2016b, Brank *et al.* 1998), and including the master slave joint constraint.

The deformed configuration and generalized strain measures are defined in Eqs. (2) and (4).

The stress resultants and moment can be defined in the deformed configuration as

$$\begin{cases} \boldsymbol{n} = N\boldsymbol{t}_1 + T\boldsymbol{t}_2 \\ m = M\boldsymbol{t}_3 \end{cases} \tag{44}$$

where $\boldsymbol{n}, m$: are work conjugate to $\boldsymbol{\varepsilon}, k$, respectively. It is important to note that, $\boldsymbol{n}, m$ are the spatial object defined in the deformed configuration, but parameterized by the coordinate set in the initial configuration. They are equivalent to the stress resultants of the first Piola-Kirchhoff stress tensor (Ibrahimbegovic and Frey 1993a).

The material objects of stress resultants and strain measures are given by

$$\boldsymbol{N} = \boldsymbol{\Lambda}^T\boldsymbol{n}, \boldsymbol{\Sigma} = \boldsymbol{\Lambda}^T\boldsymbol{\varepsilon} \tag{45}$$

$$M = m, K = k \tag{46}$$

where $\boldsymbol{N} = N\boldsymbol{t_1} + T\boldsymbol{t_2}$and $\boldsymbol{\Sigma} = \begin{pmatrix} \Sigma \\ \Gamma \end{pmatrix}$

By considering the linear elastic constitutive relation, the material objects of stress resultant and moment are given by

$$\begin{pmatrix} N \\ T \end{pmatrix} = \boldsymbol{C}\begin{pmatrix} \Sigma \\ \Gamma \end{pmatrix}, \quad M = C_m k \ ; \boldsymbol{C} = \begin{pmatrix} EA & 0 \\ 0 & GA \end{pmatrix}, C_m = EI \tag{47}$$

where E is the Young modulus, G is the shear modulus, A is the beam cross section and I is the inertia of the section.

The weak form of the equations of beam large motion is obtained as

$$\int_0^{\mathrm{L}} (\delta\boldsymbol{\varepsilon}.\,\mathbf{n} + \delta\mathrm{k}.\,\mathrm{m})\mathrm{ds} + \int_0^{\mathrm{L}} \left(\delta\boldsymbol{\varphi}.\,\mathrm{A}_\rho\ddot{\boldsymbol{\varphi}} + \delta\psi.\,\mathrm{I}_\rho\ddot{\psi}\right)\mathrm{ds} - \delta\Pi_{\mathrm{ext}} = 0 \tag{48}$$

where $\ddot{\boldsymbol{\varphi}}, \ddot{\psi}$ are the acceleration components, ($A_\rho = \int \rho dA$ and $J_\rho = \int \rho\zeta^2 dA$ are inertia coefficients. $\delta\Pi_{\mathrm{ext}}$ is the virtual work of external forces.

The virtual strains$\delta\boldsymbol{\varepsilon}$, $\delta k$are obtained by using the Lie derivative formalism (Ibrahimbegovic 2009). The variations of spatial objects are computed in initial configuration, followed by the push-forward of the result to the deformed configuration (Ibrahimbegovic and Mamouri 1999). Accordingly, the axial and shear virtual strains can be written as

$$\delta\boldsymbol{\varepsilon} = \boldsymbol{\Lambda}\delta(\boldsymbol{\Lambda}^T\boldsymbol{\varepsilon}) = \boldsymbol{\delta\varphi}' - \boldsymbol{W\varphi}'\delta\psi \tag{49}$$

where $\delta\boldsymbol{\varphi}$, $\delta\psi$ are respectively the virtual displacement and the virtual rotation.

Due to the planar nature of problem, the virtual bending strain is computed in simple way, using the identity tensor for pull-back and push-forward as follows

$$\delta k = \boldsymbol{I}\delta(\boldsymbol{I}k) = \delta\psi' \tag{50}$$

3.2.1 Finite element approximations

By using the simplest finite element interpolations based upon two node elements defined in

(6), the weak form of equation of motion in (47) can be recast in term of a set of nonlinear algebraic equations (see Mamouri *et al.* 2016b)

$$\boldsymbol{G}^{h}(.) = \boldsymbol{A}_{e=1}^{Nel}\boldsymbol{G}^{e}(.) \tag{51}$$

where $\boldsymbol{A}_{e=1}^{Nel}$ denotes the finite element assembly procedure. The weak form contribution of typical element $\boldsymbol{G}^{\boldsymbol{e}}(.)$ can be obtained as

$$\boldsymbol{G}^{e}(\boldsymbol{\varphi}^{a}, \psi^{\boldsymbol{a}}, \boldsymbol{\delta\varphi}^{a}, \delta\psi^{a}) = \sum_{a=1}^{2} \begin{pmatrix} \boldsymbol{\delta\varphi}^{a} \\ \delta\psi^{a} \end{pmatrix} . \begin{pmatrix} \widetilde{\boldsymbol{n}}^{a} \\ \widetilde{m}^{a} \end{pmatrix} \tag{52}$$

where

$$\widetilde{\boldsymbol{n}}^{a} = \int_{0}^{l^{e}} \left(\boldsymbol{N}_{a}'\boldsymbol{n} + \boldsymbol{N}_{a}\mathrm{A}_{\rho}\ddot{\boldsymbol{\varphi}}^{a} \right) \boldsymbol{ds} - \boldsymbol{n}_{ext}^{a} \tag{53}$$

$$\widetilde{m}^{a} = \int_{0}^{l^{e}} \left(\boldsymbol{N}_{a}'m - \boldsymbol{N}_{a}(\mathbf{W}\boldsymbol{\varphi}').\boldsymbol{n} + \boldsymbol{N}_{a}\mathrm{I}_{\rho}\ddot{\psi}^{a} \right) \boldsymbol{ds} - m_{ext}^{a} \tag{54}$$

with $\boldsymbol{n}_{ext}^{a}$ and m_{ext}^{a} are external nodal forces and moments. We apply the master slave approach, and consider node a in the element e as slave node whose motion is governed by the motion of the master node m with respect to the revolute joint constraint (see Ibrahimbegovic and Mamouri 2000); the modified contribution of an element to the weak form of equation of motion can be written, starting from (51), in term of master node motion, as

$$\boldsymbol{G}^{\boldsymbol{e}}(\boldsymbol{\varphi}^{b}, \psi^{\boldsymbol{b}}, \boldsymbol{\varphi}^{m}, \psi^{m}, \psi^{r}, \delta\boldsymbol{\varphi}^{b}, \delta\psi^{b}, \delta\boldsymbol{\varphi}^{m}, \delta\psi^{m}, \delta\psi^{r}) = \begin{pmatrix} \boldsymbol{\delta\varphi}^{m} \\ \delta\psi^{m} \\ \boldsymbol{\delta\varphi}^{b} \\ \delta\psi^{b} \end{pmatrix} . \begin{pmatrix} \widetilde{\boldsymbol{n}}^{s} \\ \widetilde{m}^{s} \\ \widetilde{\boldsymbol{n}}^{b} \\ \widetilde{m}^{b} \end{pmatrix} + \begin{pmatrix} 0 \\ \delta\psi^{r} \end{pmatrix} . \begin{pmatrix} \widetilde{\boldsymbol{n}}^{s} \\ \widetilde{m}^{s} \end{pmatrix} \tag{55}$$

3.3 Energy conserving\decaying time integration scheme

In this section we discuss shortly the time integration schemes designed for controllable energy conservation or decay to overcome the loss of accuracy especially for the computed internal forces in presence of the high frequency contribution that can be resolved by reasonably coarse finite element mesh.

This scheme is based on the mid-point rule approximation. This concept is used for time derivation of weak form, which should be written at middle of time step increment (Ibrahimbegovic and Mamouri 2002, Brank *et al.* 1998) $t_{n+1/2} = t_{n} + \frac{\Delta t}{2}$, where $\Delta t = t_{n+1} - t_{n}$, as

$$\begin{aligned} &\int_{0}^{L} \left((\boldsymbol{\delta\varphi}' - \boldsymbol{W\varphi}'\delta\psi).\boldsymbol{n}_{n+\frac{1}{2}} + \delta\psi'.m_{n+\frac{1}{2}} \right) ds + \\ &\int_{0}^{L} \left(\delta\boldsymbol{\varphi}.A_{\rho}\ddot{\boldsymbol{\varphi}}_{n+\frac{1}{2}} + \delta\psi.I_{\rho}\ddot{\psi}_{n+\frac{1}{2}} \right) ds - \delta\Pi_{n+\frac{1}{2}}^{ext} = 0 \end{aligned} \tag{56}$$

The displacement and rotation, at the middle of time step are computed as

$$\begin{cases} \boldsymbol{\varphi}_{n+1/2} = \dfrac{\boldsymbol{\varphi}_{n+1} + \boldsymbol{\varphi}_n}{2} \\ \psi_{n+1/2} = \dfrac{\psi_{n+1} + \psi_n}{2} \end{cases} \tag{57}$$

when using this approach, we note that the rotation matrix is orthogonal (see Mamouri *et al.* 2016a), when described at the middle of time step as

$$\boldsymbol{\Lambda}_{n+1/2} = \begin{bmatrix} cos\,\psi_{+1/2} & -sin\,\psi_{+1/2} \\ sin\,\psi_{+1/2} & cos\,\psi_{+1/2} \end{bmatrix} \tag{58}$$

For the energy decaying scheme, the constitutive equations and update of velocities are constructed in the manner that ensures that the energy will be dissipated by filtering out the high frequency contribution over each time step where it needed. The latter is achieved by using two control parameters for internal and kinetic energy, and the algorithmic constitutive equations as

$$\boldsymbol{N}_{n+\frac{1}{2}} = \boldsymbol{C}\frac{1}{2}(\boldsymbol{\Sigma}_{n+1} + \boldsymbol{\Sigma}_n) + \alpha(\boldsymbol{\Sigma}_{n+1} - \boldsymbol{\Sigma}_n) \tag{59}$$

$$M_{n+\frac{1}{2}} = C_m(K_{n+1} + K_n) + \alpha(K_{n+1} + K_n) \tag{60}$$

where $\alpha \in \left[0\,, \frac{1}{2}\right]$ is the internal energy dissipation parameter.

In order to ensure the decay of the total energy in the case of vanishing strains, we ought to introduce dissipation in the inertia term, resulting with an appropriate velocity modification by adding the corresponding dissipation term. The update of velocities can be performed by using

$$\begin{cases} \dfrac{\boldsymbol{\varphi}_{\mathrm{n}+1} - \boldsymbol{\varphi}_{\mathrm{n}}}{\Delta t} = \dot{\boldsymbol{\varphi}}_{\mathrm{n}+1/2} + \beta(\dot{\boldsymbol{\varphi}}_{\mathrm{n}+1} + \dot{\boldsymbol{\varphi}}_{\mathrm{n}}) \\ \dfrac{\psi_{\mathbf{n}+1} - \psi_{\mathrm{n}}}{\Delta t} = \dot{\psi}_{\mathrm{n}+1/2} + \beta(\dot{\psi}_{\mathrm{n}+1} + \dot{\psi}_{\mathrm{n}}) \end{cases} \tag{61}$$

with $\beta \in \left[0\,, \frac{1}{2}\right]$ is the kinetic energy dissipation parameter.

With the controllable parameters $\alpha\ and\ \beta$, the scheme proposed is able to dissipate the energy with filtering out the high frequency contribution. With the choice of parameters:$\alpha = \beta = 0$, the dissipation terms are equal to zero, which leads to energy conserving scheme preserving the total energy.

For more details about the energy conserving/decaying scheme, we refer to (Mamouri *et al.* (2016a) and (Ibrahimbegovic and Mamouri 2002).

Linearization and computational procedure:

Using the expressions of velocity and acceleration update, the weak form of equation of motion in (56) can be written as an explicit function of the nodal displacements and rotations at time $\mathrm{t_{n+1}}$

$$\begin{aligned} &\boldsymbol{G}(\boldsymbol{\varphi}_{\mathrm{n}+1,\epsilon}, \psi_{\mathbf{n}+1,\epsilon}, \delta\boldsymbol{\varphi}, \delta\psi) = \\ &\int_0^L \left(\delta\boldsymbol{\varphi}.A_\rho\left[\frac{2}{\Delta t^2}(\boldsymbol{\varphi}_{n+1,\epsilon} - \boldsymbol{\varphi}_n) - \frac{2}{\Delta t}\dot{\boldsymbol{\varphi}}_n\right]\right)ds + \int_0^L \left(\delta\psi.I_\rho\left[\frac{2}{\Delta t^2}(\psi_{\boldsymbol{n}+1,\epsilon} - \psi_{\boldsymbol{n}}) - \frac{2}{\Delta t}\dot{\psi}_{\boldsymbol{n}}\right]\right)ds \\ &+ \int_0^L \left(\left(\delta\boldsymbol{\varphi}' - \boldsymbol{W}\boldsymbol{\varphi}'\delta\psi\right).\frac{1}{2}\boldsymbol{\Lambda}^T_{n+\frac{1}{2}}\boldsymbol{C}\left(\boldsymbol{\Lambda}^T_{n+1}\boldsymbol{\varphi}'_{n+1,\epsilon} + \boldsymbol{\Lambda}^T_n\boldsymbol{\varphi}'_n - \boldsymbol{t}_2\right)\right)ds \\ &+ \int_0^L \left(\delta\psi'.\frac{1}{2}C_m\left(\psi'_{n+1,\epsilon} + \psi'_n\right)\right)ds - \delta\Pi^{ext}_{\boldsymbol{n}+\frac{1}{2}} = 0 \end{aligned} \tag{62}$$

The linearized form of the result (62) can be obtained by consistent linearization (Ibrahimbegovic 2009)

$$\boldsymbol{Lin}\left(\boldsymbol{G}\left(\boldsymbol{\varphi}_{\mathrm{n}+\frac{1}{2}},\psi_{\mathrm{n}+\frac{1}{2}},\delta\boldsymbol{\varphi},\delta\psi\right)\right)=\boldsymbol{G}_{\mathrm{n}+\frac{1}{2}}+\frac{d}{d\epsilon}\Big|_{\epsilon=0}\left[\boldsymbol{G}(\boldsymbol{\varphi}_{\mathrm{n}+1,\boldsymbol{\epsilon}},\psi_{\mathrm{n}+1,\epsilon},\delta\boldsymbol{\varphi},\delta\psi)\right] \tag{63}$$

where

$$\begin{cases}\boldsymbol{\varphi}_{\mathrm{n}+1,\epsilon}=\boldsymbol{\varphi}_{\mathrm{n}+1}+\ \epsilon\Delta\boldsymbol{\varphi}_{\mathrm{n}+1}\\ \psi_{\mathrm{n}+1,\epsilon}=\psi_{\mathrm{n}+1}+\ \epsilon\Delta\psi_{\mathrm{n}+1}\end{cases} \tag{64}$$

with $\boldsymbol{\varphi}_{\mathrm{n}+1}$, $\psi_{\mathrm{n}+1}$ are respectively the incremental displacements and rotations. The second term in (63) can be written as

$$\frac{\boldsymbol{d}}{\boldsymbol{d\epsilon}}\Big|_{\boldsymbol{\epsilon=0}}\left[\boldsymbol{G}_{\mathrm{n}+\frac{1}{2},\boldsymbol{\epsilon}}\right]=\int_{\boldsymbol{0}}^{\boldsymbol{l^e}}\begin{pmatrix}\boldsymbol{\delta\varphi}\\ \delta\psi\end{pmatrix}[\boldsymbol{H}].\begin{pmatrix}\Delta\boldsymbol{\varphi}_{\mathrm{n}+1}\\ \Delta\psi_{\mathrm{n}+1}\end{pmatrix}\boldsymbol{ds}\ +\int_{\boldsymbol{0}}^{\boldsymbol{l^e}}\begin{pmatrix}\boldsymbol{\delta\varphi'}\\ \delta\psi\\ \delta\psi'\end{pmatrix}.[\boldsymbol{D}]\begin{pmatrix}\Delta\boldsymbol{\varphi'}_{\mathrm{n}+1}\\ \Delta\psi_{\mathrm{n}+1}\\ \Delta\psi'_{\mathrm{n}+1}\end{pmatrix}\boldsymbol{ds} \tag{65}$$

with

$$[\boldsymbol{D}]=[\boldsymbol{E}+\boldsymbol{G}]$$

The explicit forms of the matrices $[\boldsymbol{H}],[\boldsymbol{E}]and[\boldsymbol{G}]$ are given below. With the respect to the joint constraint, considering node *a* as a slave node s whose motion can be governed by the master node m motion and relative displacement and rotation, the discretized form of (65) can be written as

$$\begin{aligned}\frac{d}{d\epsilon}\Big|_{\epsilon=0}\left[\boldsymbol{G}_{\mathrm{n}+\frac{1}{2},\epsilon}\right]=&\begin{pmatrix}\boldsymbol{\delta\varphi}_b\\ \delta\psi_b\\ \boldsymbol{\delta\varphi}_m\\ \delta\psi_m\end{pmatrix}.\left[\widehat{\boldsymbol{K}}\right]\begin{pmatrix}\Delta\boldsymbol{\varphi}^b_{n+1}\\ \Delta\psi^b_{n+1}\\ \Delta\boldsymbol{\varphi}^m_{n+1}\\ \Delta\psi^m_{n+1}\end{pmatrix}+\begin{pmatrix}\boldsymbol{\delta\varphi}_b\\ \delta\psi_b\\ \boldsymbol{\delta\varphi}_m\\ \delta\psi_m\end{pmatrix}.\left[\widehat{\boldsymbol{F}}\right]\Delta\psi^{\boldsymbol{r}}_{\boldsymbol{n+1}}\ +\delta\psi_{\boldsymbol{r}}\left[\widehat{\boldsymbol{G}}\right]\begin{pmatrix}\Delta\boldsymbol{\varphi}^b_{n+1}\\ \Delta\psi^b_{n+1}\\ \Delta\boldsymbol{\varphi}^m_{n+1}\\ \Delta\psi^m_{n+1}\end{pmatrix}\\ &+\delta\psi_r\left[\widehat{\boldsymbol{H}}\right]\Delta\psi^r_{n+1}\end{aligned} \tag{66}$$

Where

$$\left[\widehat{\boldsymbol{K}}\right]=\int_{\boldsymbol{0}}^{\boldsymbol{l^e}}([\boldsymbol{B}_{iner}]^T[\boldsymbol{H}][\boldsymbol{B}_{iner}])\,ds+\int_{\boldsymbol{0}}^{\boldsymbol{l^e}}([\boldsymbol{B}_{int}]^T[\boldsymbol{D}][\boldsymbol{B}_{int}])\,ds$$

$$\left[\widehat{\boldsymbol{F}}\right]=\int_{\boldsymbol{0}}^{\boldsymbol{l^e}}([\boldsymbol{B}_{iner}]^T[\boldsymbol{H}][\boldsymbol{B}_{1r}])\,ds+\int_{\boldsymbol{0}}^{\boldsymbol{l^e}}([\boldsymbol{B}_{int}]^T[\boldsymbol{D}][\boldsymbol{B}_{2r}])\,ds$$

$$\left[\widehat{\boldsymbol{G}}\right]=\int_{\boldsymbol{0}}^{\boldsymbol{l^e}}([\boldsymbol{B}_{1r}]^T[\boldsymbol{H}][\boldsymbol{B}_{iner}])\,ds+\int_{\boldsymbol{0}}^{\boldsymbol{l^e}}([\boldsymbol{B}_{2r}]^T[\boldsymbol{D}][\boldsymbol{B}_{int}])\,ds$$

$$\left[\widehat{\boldsymbol{H}}\right]=\int_{\boldsymbol{0}}^{\boldsymbol{l^e}}\left([\boldsymbol{B}_{1r}]^{\boldsymbol{T}}[\boldsymbol{H}][\boldsymbol{B}_{1r}]\right)ds+\int_{\boldsymbol{0}}^{\boldsymbol{l^e}}\left([\boldsymbol{B}_{2r}]^{\boldsymbol{T}}[\boldsymbol{D}][\boldsymbol{B}_{2r}]\right)ds$$

$[\boldsymbol{B}_{iner}],[\boldsymbol{B}_{int}],[\boldsymbol{B}_{1r}]\ \boldsymbol{and}\ [\boldsymbol{B}_{2r}]$ are given as

$$[\boldsymbol{B}_{iner}] = \begin{bmatrix} \boldsymbol{N}_b & \boldsymbol{0} & \boldsymbol{N}_s\ 0 \\ 0 & N_b & 0\ N_s \end{bmatrix}; [\boldsymbol{B}_{1r}] = \begin{bmatrix} 0 \\ N_s \end{bmatrix}$$

$$[\boldsymbol{B}_{int}] = \begin{bmatrix} \boldsymbol{N}_b' & 0 & \boldsymbol{N}_s'\ 0 \\ \boldsymbol{0} & N_b & \boldsymbol{0}\ N_s \\ \boldsymbol{0} & N_b' & \boldsymbol{0}\ N_s' \end{bmatrix}; [\boldsymbol{B}_{2r}] = \begin{bmatrix} 0 \\ N_s \\ N_s' \end{bmatrix}$$

Since the additional relative variables are assigned to a particular element only, they can be handled locally by using the static condensation procedure. For that, the relative incremental rotation vector can be written as

$$\Delta\psi_{\boldsymbol{n+1}}^{\boldsymbol{r}} = -\left[\widehat{\boldsymbol{H}}\right]^{-\boldsymbol{1}}\left[\widehat{\boldsymbol{G}}\right]\begin{pmatrix} \Delta\boldsymbol{\varphi}_{\boldsymbol{n+1}}^{\boldsymbol{b}} \\ \Delta\psi_{\boldsymbol{n+1}}^{\boldsymbol{b}} \\ \Delta\boldsymbol{\varphi}_{\boldsymbol{n+1}}^{\boldsymbol{m}} \\ \Delta\psi_{\boldsymbol{n+1}}^{\boldsymbol{m}} \end{pmatrix} \tag{67}$$

By replacing the last result in (67), we obtain the condensed form of tangent stiffness matrix by

$$\left[\widetilde{\boldsymbol{K}}\right] = \left[\widehat{\boldsymbol{K}}\right] - \left[\widehat{\boldsymbol{F}}\right]\left[\widehat{\boldsymbol{H}}\right]^{-1}\left[\widehat{\boldsymbol{G}}\right] \tag{68}$$

This Tangent matrix will be used to define the corresponding displacement increment and update for new displacement.

4. Contact problem governing equations

Considering complete collapse of a structure, we need finally to describe its contact with the ground. To that end, we provide here a short description of contact problem and its governing equations. We only consider the frictionless case, which is sufficient to obtain the structure debris dispersion.

4.1 Kinematic

We consider the cantilever beam which can be enter in contact with a rigid obstacle as presented in Fig. 6. Initially, the distance between the beam free end and the rigid obstacle is defined by g_0. In subsequent deformed configuration, the new distance to the obstacle is g_t.

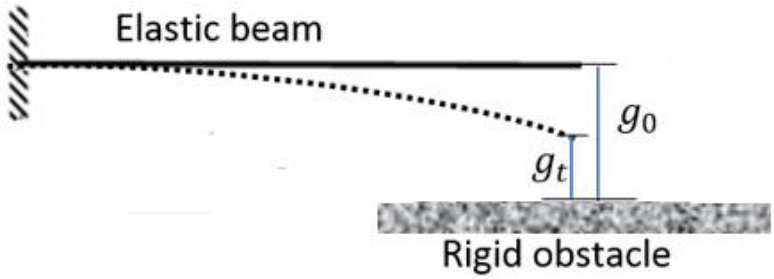


Fig. 6 Contact of beam with rigid obstacle

The chosen sign convention implies that this distance can be either positive, if there is no contact, or zero, when the beam is in contact with obstacle

$$\mathrm{g_t} \geq 0 \tag{69}$$

With the respect to the action-reaction principle, the rigid obstacle produces a reaction opposite to the beam action. The latter can be positive, in the case of contact, and zero otherwise.

$$\bar{\mathrm{p}}_\mathrm{t} \geq 0 \tag{70}$$

The contact constrains can be written in term of the Kuhn-Tucker condition as

$$\mathrm{g_t}.\bar{\mathrm{p}}_\mathrm{t} = 0 \tag{71}$$

It means that always one between the contact gap $\mathrm{g_t}$and the reaction contact $\bar{\mathrm{p}}_\mathrm{t}$ is equal to zero.

4.2 Penalty method for contact problem

The contact problem described previously is here handled by the penalty method (Ibrahimbegovic 2009). The simple quadratic penalty function can be written in standard way

$$P(g_t) = \begin{cases} \frac{1}{2}k(g_t)^2 g_t \geq 0 \\ 0 \qquad\qquad g_t < 0 \end{cases} \tag{72}$$

Where k is the chosen penalty parameters. The use of this penalty function is equivalent to considering the rigid obstacle as an elastic spring with elasticity coefficient equal to k (see Ibrahimbegovic 2009 for more details). The contact force can be written in term of displacement as

$$\bar{\mathrm{p}}_\mathrm{t} = \begin{cases} k(g_t) & g_t \geq 0 \\ 0 & g_t < 0 \end{cases} \tag{73}$$

Using the mid-point scheme, the contact force can be written in term of conservation as

$$p_{\mathrm{cons}} = k\frac{1}{2}(g_{n+1} + g_n) \tag{74}$$

In order to take into account, the effect of dissipation, we introduce the parameter α

$$p_{\mathrm{diss}} = p_{\mathrm{cons}} + \alpha k(g_{n+1} - g_n) \tag{75}$$

4.3 Motion equations with contact using energy conserving\decaying scheme

The time integration of equation of motion is done using the mid-point scheme. The equations to solve can be obtained starting from the linearized form in (66), and considering the contact of structure with the ground at$t_{n+1/2} = t_n + \frac{\Delta t}{2}$

$$\begin{aligned}\left(\left[\widetilde{\boldsymbol{K}}\right]_{n+\frac{1}{2}}^{i-1} + \boldsymbol{K}_{n+\frac{1}{2}}^{contact,i-1}\right)\Delta\boldsymbol{u}_{n+1}^{i} = \boldsymbol{F}_{n+\frac{1}{2}}^{ext} - \boldsymbol{F}_{\left(n+\frac{1}{2}\right)}^{int(i-1)} - \boldsymbol{F}_{n+\frac{1}{2}}^{contact,(i-1)} \\ - \boldsymbol{M}\left(\frac{2}{\Delta t^2}\left(\mathbf{u}_{\mathrm{n+1}}^{\mathrm{i-1}} - \mathbf{u}_{\mathrm{n}}\right) - \frac{2}{\Delta t}\dot{\mathbf{u}}_{\mathrm{n}}\right)\end{aligned} \tag{76}$$

where, $\left[\widetilde{\boldsymbol{K}}\right]$ is the condensed matrix defined in (71), $\boldsymbol{F}_{n+\frac{1}{2}}^{contact,(i-1)}$ is the contact residual and $\boldsymbol{K}_{n+\frac{1}{2}}^{contact,i-1}$ is the linearized contact stiffness matrix, $\boldsymbol{M}$ is the mass matrix, $\Delta\boldsymbol{u}_{n+1}^{i}$ is the incremental displacement and rotation vector. The equations of mid-point rule are computed using the same updates as used before in (57) and (61). By solving the Eq. (76), we get the incremental displacements and new values of displacements, which allow us to compute the new values of velocities and accelerations

4. Numerical examples

All the computations in this work are performed by a research version of FEAP program (see Zienkiewicz and Taylor 2005). To illustrate the efficiency of proposed models for different phases of collapse simulations, several numerical examples are presented in Jukic *et al.* (2013).

• The cantilever beam and two-story frame are used to illustrate the efficiency of the model. The Static analysis of failure is used.

• The six-story building is used explain the methodology for complete Progressive collapse of construction.

5.1 Cantilever beam

We consider the cantilever beam of rectangular cross section with length L = 2.5 m, three loading cases at the end of the cantilever beam are tested.

The geometric and material proprieties are chosen as: $EI = 77650\,KNm^2$, $M_c = 37.9\,KNm$, $M_y = 268\,KNm$, $K_{h1} = 29400\,KNm^2$, $K_{h2} = 272\,KNm^2$, $M_u = 274\,KNm$, $K_s = -18000\,KNm$.

1. The cantilever beam is loaded at the free end by a moment (Fig. 7).

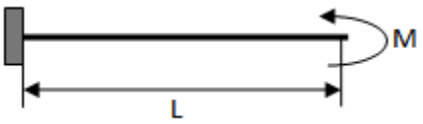


Fig. 7 Cantilever beam with end moment

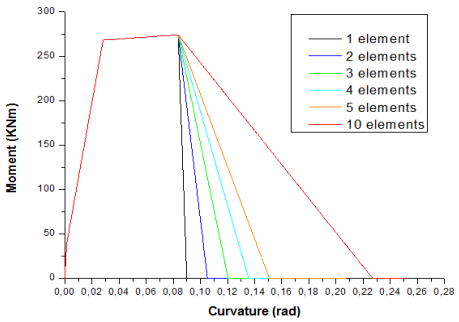


Fig. 8 Cantilever beam with end moment: Different number of elements

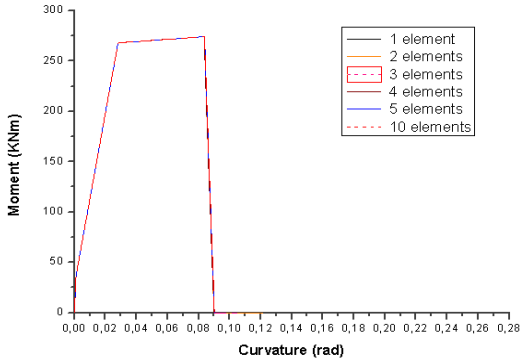


Fig. 9 Cantilever beam with end moment: Different number of elements with one weakened

2. The second load case of the cantilever beam concerns the free end moment and axial force applied simultaneously (Fig. 10), which is representative of conditions for a column.

The material parameters chosen for this example are:$N = 100\ KNm$,$M_c = 55\ KNm$, $M_y = 395\ KNm$,$K_{h1} = 35000\ KNm^2$, $K_{h2} = 352\ KNm^2$, $M_u = 401\ KNmK_s = -26000\ KN$

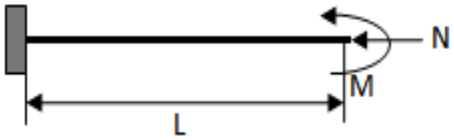


Fig. 10 Cantilever beam with end moment and constant axial force

Fig. 11 shows the deference obtained in cantilever beam response in failure analysis, with and without axial force.

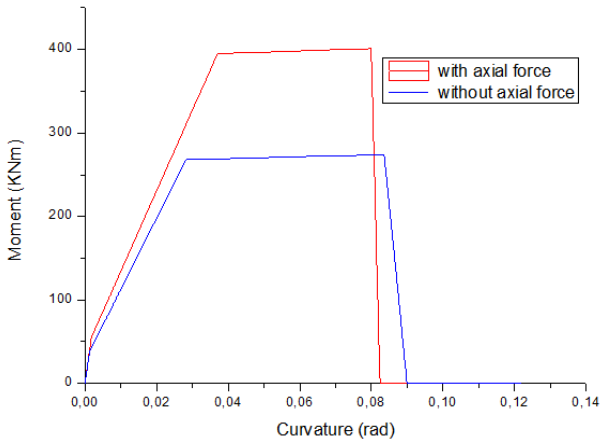


Fig. 11 Cantilever beam response under end moment with and without axial force

3. Third load case of the cantilever beam concerns the free end vertical force. We use the same geometric and material proprieties as for load case 1, except the ultimate moment value where we use$M_u = 374\ KNm$. (Fig. 12).

The cantilever beam is modeled with 10, 15, 20 and 25 finite elements. An imposed vertical displacement is applied at the free end in order to get the failure analysis.

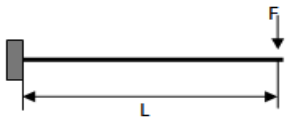


Fig. 12 Cantilever beam under transversal force

Fig. 13 shows that the different mesh grading presents the same slope softening but not the same ultimate load. This difference can appear from the use of only one integration point, which leads to a shift of the plastic hinge. In this example, there is no need for weakening one of finite elements, because the nature of problem presents non-homogeneous stress state.

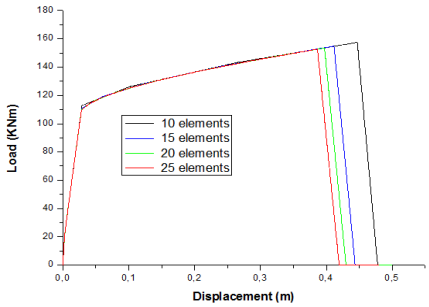


Fig. 13 Cantilever beam response under transversal force: Different mesh

5.2 Two-story reinforced concrete frame

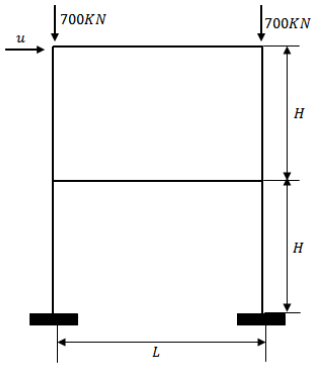


Fig. 14 Two-story frame

We consider two-story reinforced concrete frame with height H =2 m and span L =3.5 m. Columns and beams have the same rectangular cross section$b \times h = 0.3 \times 0.4\, m^2$. The material proprieties needed for computation are given by (see Dujc *et al.* 2010).

$M_c = 100\ KNm;\ M_y = 245\ KNm;\ M_u = 265\ KNm;\ K_{h1} = 12450\ KNm^2;\ K_{h2} = 195\ KNm^2;\ K_s = -2410\ KNm$ for columns.

$M_c = 30\ KNm;\ M_y = 150\ KNm;\ M_u = 170\ KNm;\ K_{h1} = 11190\ KNm^2;\ K_{h2} = 137\ KNm^2;\ K_s = -1310\ KNm$ for beams.

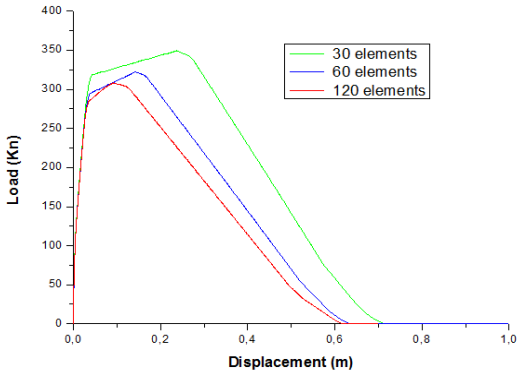


Fig. 15 Response of the frame up to the total collapse using different mesh

Columns are clamped at the bottom. The load is applied in two steps. First, constant vertical force act at the top of both columns. Second, we impose horizontal displacement u at the left top of the frame.

The structure is modeled by 30, 60 and 120 finite elements. Fig. 15 shows that we get better results when increasing number of elements. The results illustrate that the model is able to predict the complete failure after creating six plastic hinges located in joints beam-column and two bottom clamped support (Fig. 16).

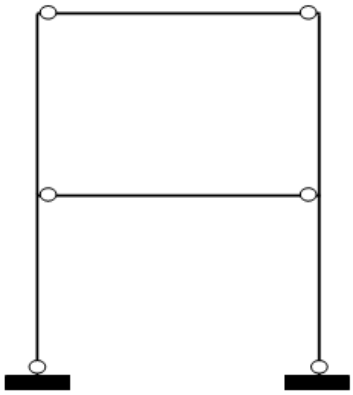


Fig. 16 plastic hinges in Two-story frame

5.3 Six-story building

We consider six-story frame with floor height H =3m and span L =4m. Columns and beams have the same rectangular cross section$b \times h = 0.3 \times 0.4\ m^2$. The material proprieties needed for computation are given by (see Imamovic *et al.* (2015) for the material proprieties identification).

$M_c = 100\ KNm;\ \ M_y = 245\ KNm;\ \ M_u = 265\ KNm;\ \ K_{h1} = 12450\ KNm^2;\ \ K_{h2} = 195\ KNm^2$for columns.

$M_c = 30\ KNm;\ \ M_y = 150\ KNm;\ \ M_u = 170\ KNm;\ \ K_{h1} = 11190\ KNm^2;\ \ K_{h2} = 137\ KNm^2$for beams.

Columns are clamped at the bottom. The frame is modeled with 84, 144 and 288 elements. The progressive collapse analysis is performed in two steps:

Step 1: static analysis is performed by considering an elasto-plasticity with bi-linear isotropic hardening followed by the softening producing the failure mechanism.

The load is applied in two steps. First, constant vertical force act at the top columns. Second, we impose horizontal displacement with function u(t), which grows linearly with the pseudo-time, at the left top of the frame.

Fig. 18 present the response of frame using different mesh. The use of 288 elements give better result than 84 and 144 elements. Fig. 19 present the response of frame using different values of the softening modulus. When we use small value of the softening modulus, the structure fails when the most of softening plastic hinges are activated. In opposite, the structure fails after that the first hinges are activated, and the rest of hinges are not activated anymore, because of redistribution of stress in frame.

A static analysis is performed using 288 elements model with softening's module $K_s = -393\ KNm$ for beam and $K_s = -723\ KNm$ for columns. Such values of softening moduli allow the creation of most plastic hinges. (Fig. 20).

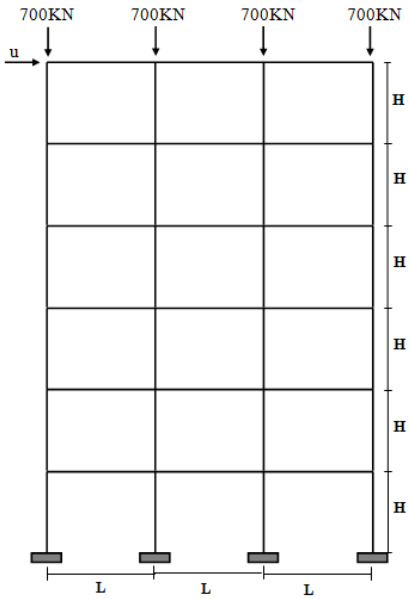


Fig. 17 Six story frame

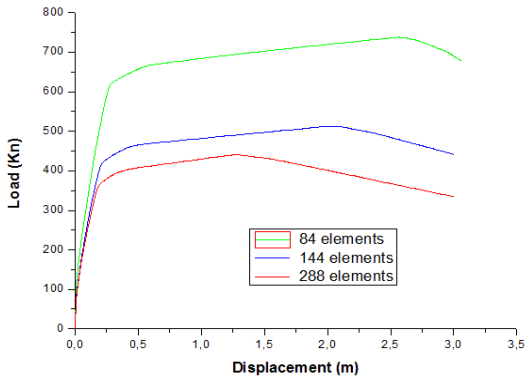


Fig. 18 Response of six story frame using different mesh

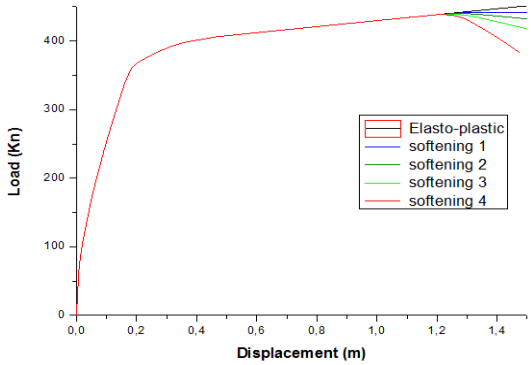


Fig. 19 Response of six story frame using different softening's modulus

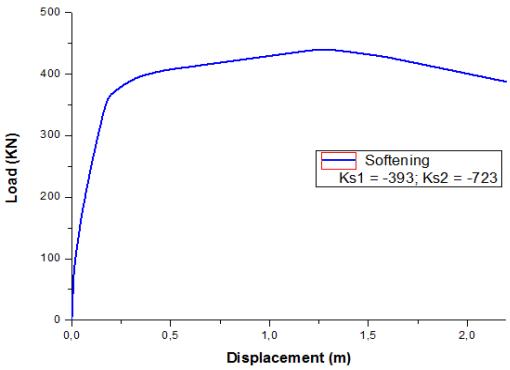


Fig. 20 Response of six-story frame up to the creation of all plastic hinges

Fig. 21 shows the locations of softening plastic hinges in the frame. It is important to note that the most of plastic hinges are formed in beams. There are only four hinges formed in clamped columns and two hinges in top columns.

A second step of the analysis is performed in order to complete the progressive collapse. A multibody system dynamic analysis is performed for six-story frame mechanism formed after the creation of the softening plastic hinges (obtained at the end of the previous analysis in the first

step). The mesh of the first step is modified by replacing all of the plastic hinges by kinematic conditions between connected nodes, for getting a hinge mechanism. We also consider the contact between the frame and the ground and assume an elastic behavior of the structural mechanism.

Both Newmark scheme and energy conserving/decaying scheme are used and compared. We impose horizontal displacement which grows linearly with time $u(t)$ at the left top of the frame, and we monitor the reaction force at the same location. We note that the gravity load is not considered in the dynamic analysis. Figs. 25 and 27 show that with Newmark scheme, the response is too far to the realistic structure behavior, due to the high frequency oscillations. In the same figures, we observe that with energy conserving scheme, the response describes a behavior better than first scheme; but the structure oscillates and it is not able to find its stable final position. However, as is shown in Figs. 26 and 28, with energy decaying scheme we are able to capture response of structure without oscillations by using values of parameters $\alpha = \beta = 0.01$, 0.1, 0.25 and 0.5, which describe the structure behavior in realistic way.

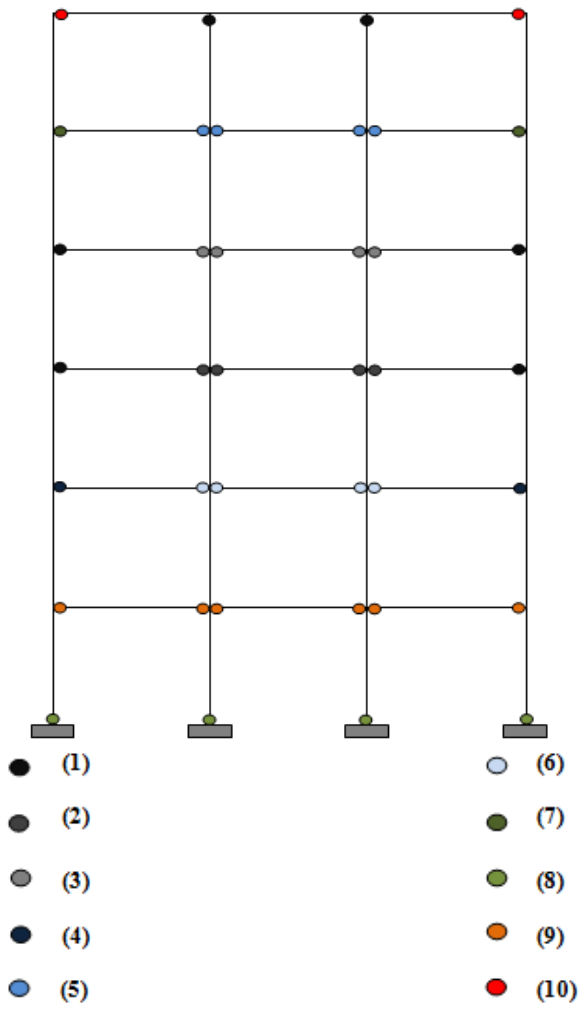


Fig. 21 Location of softening plastic hinges in six-story frame

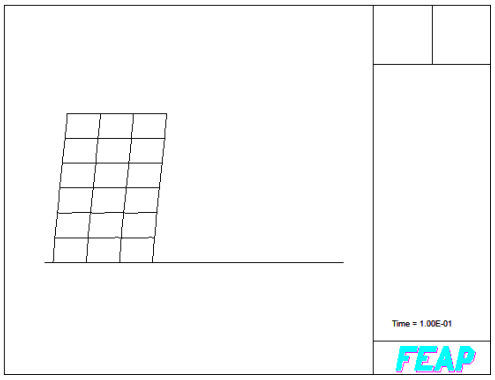


Fig. 22 Deformed shape of six story frame

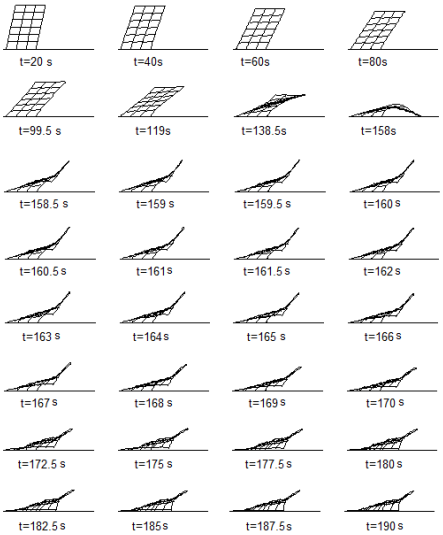
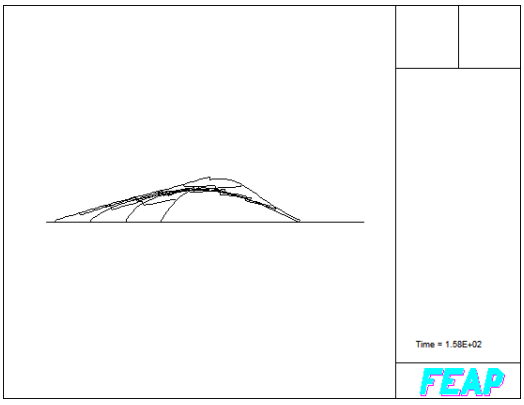
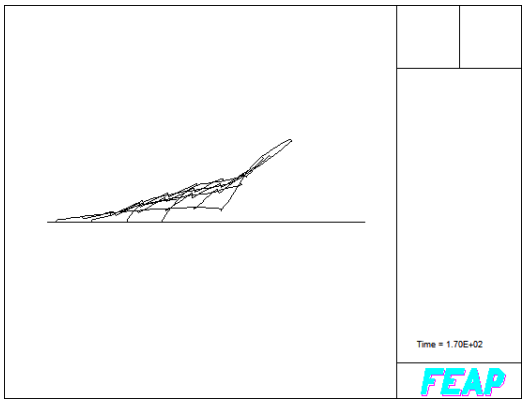


Fig. 23 Progressive collapse with contact: with conserving energy scheme (alpha= beta=0.5)

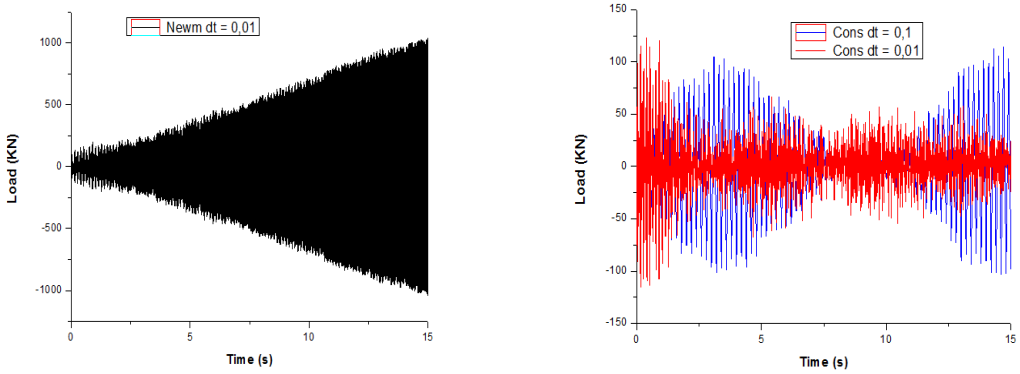


(a) frame at t = 158 s



(b) frame at t = 170 s

Fig. 24 Deformed shape of six story frame



(a) (b)

Fig. 25 Force versus Time computed by Newmark scheme (a) and energy-conserving scheme (b)

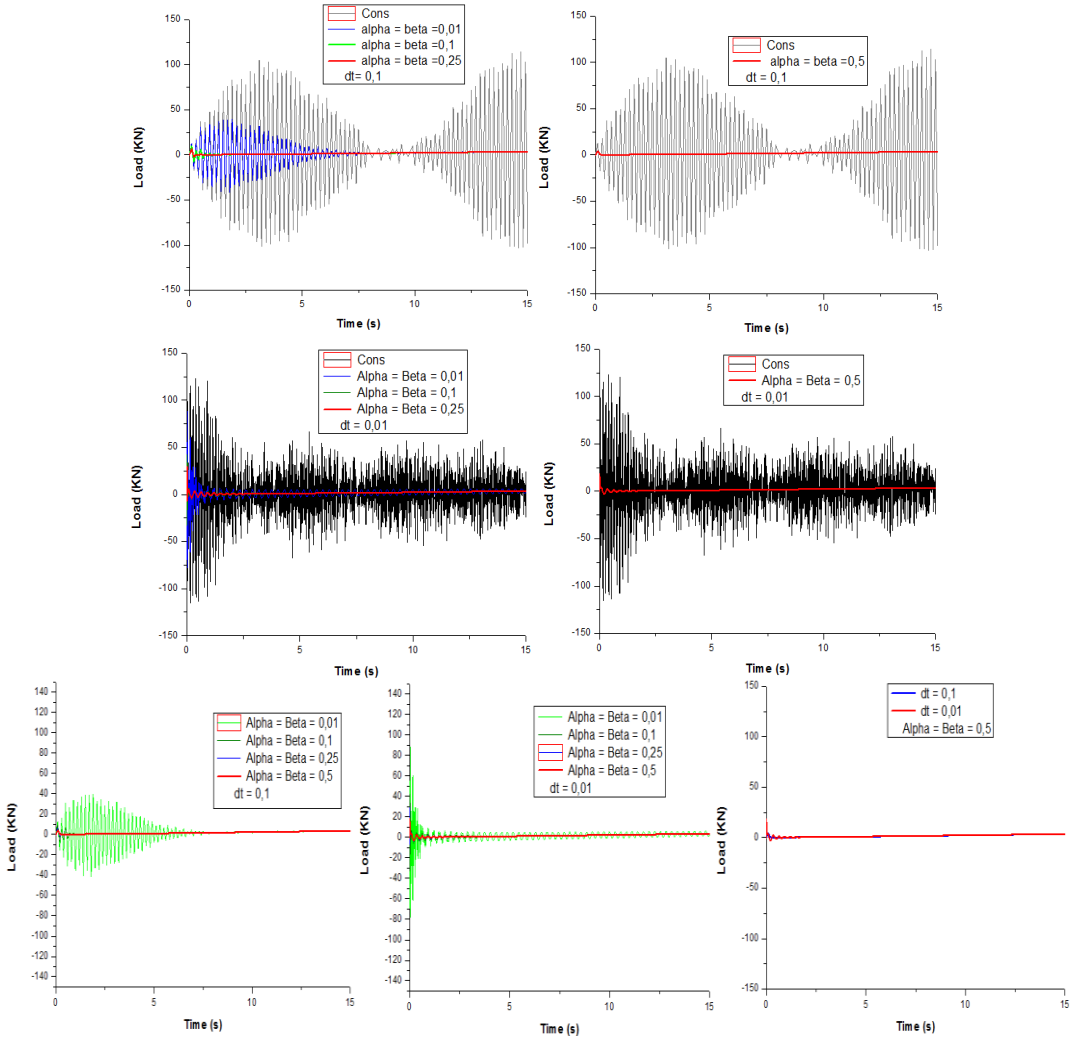
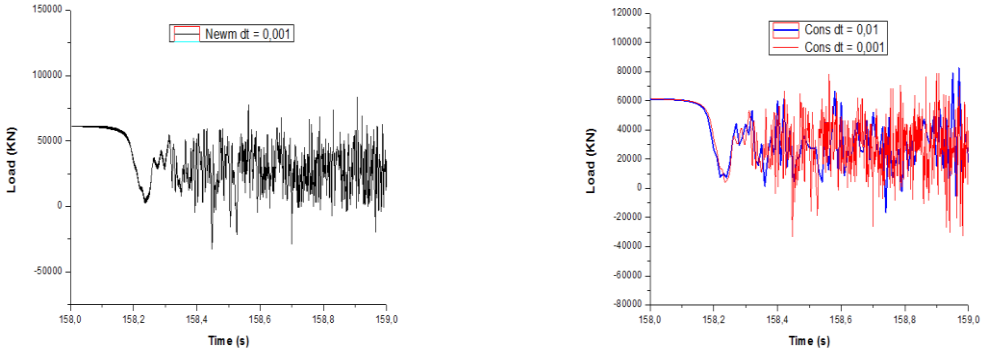


Fig. 26 Force versus Time using energy-decaying scheme



(a) (b)

Fig. 27 Force versus Time computed by Newmark scheme (a) and energy-conserving scheme (b): structure in contact with ground

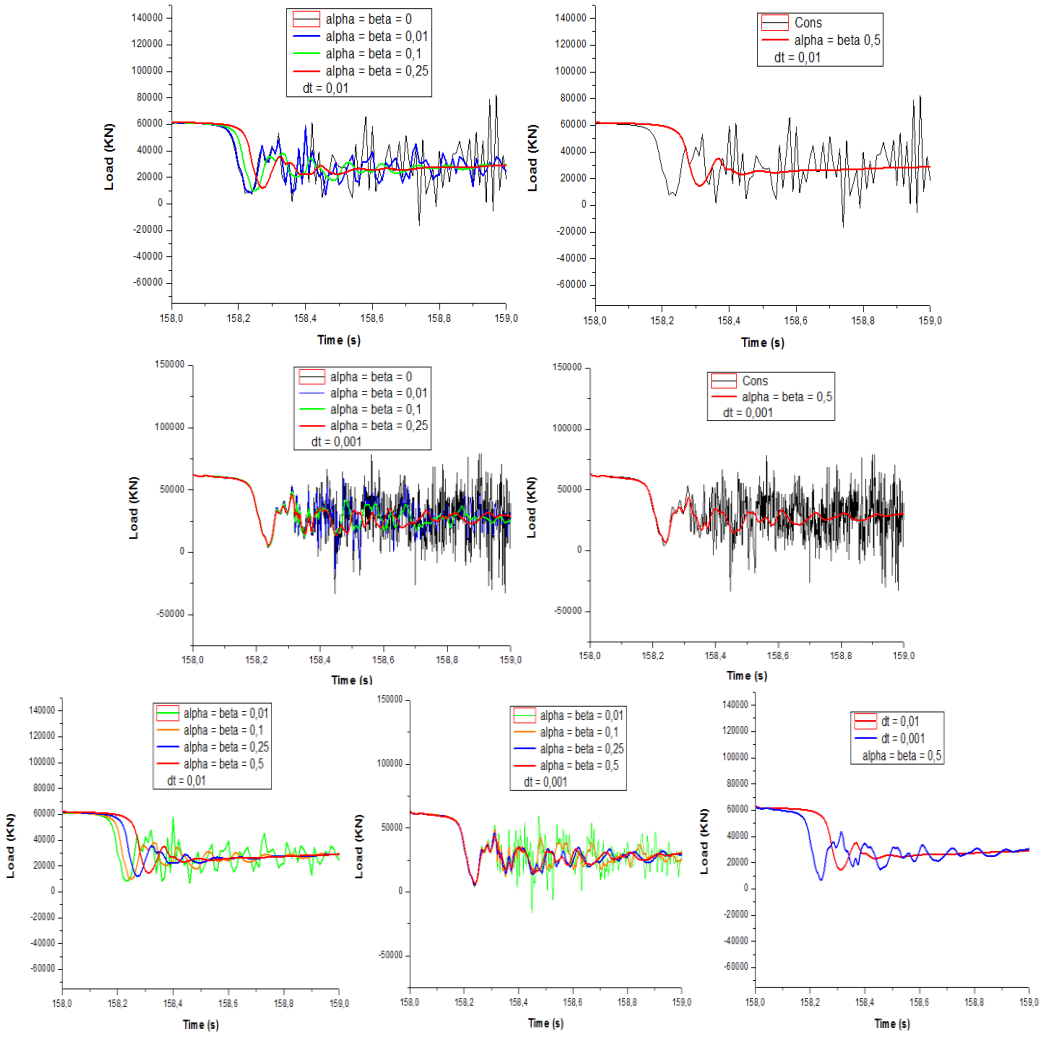


Fig. 28 Force versus Time using energy-decaying scheme: Structure in contact with ground

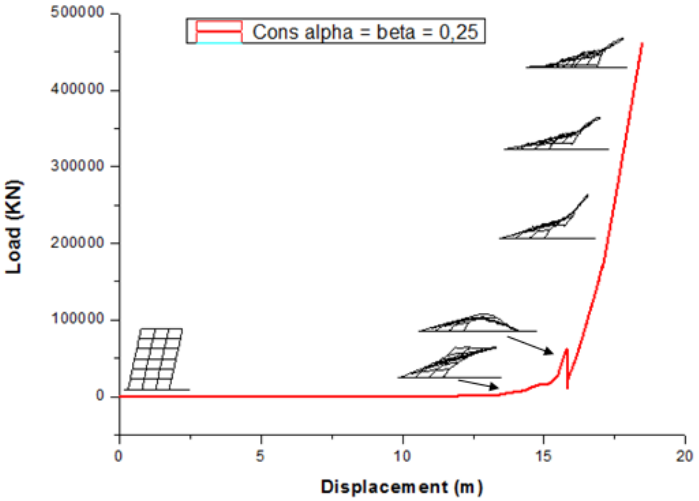


Fig. 29 Dynamic response of six-story frame until total collapse

Fig. 23 illustrates the progressive collapse of six-story frame. At time t = 170 s, the frame is completely collapsed. (Fig. 24). From Fig. 29, it is clear that, with frictionless impact consideration with the ground, the structure is pushed up again when touching the ground at t = 158 s and is shot down slowly which require larger force at final stages of the collapse; this observation can be explained by the absence of gravity load which can accelerate the demolition of structure. In other hand, the imposed loading may be not sufficient for total collapse in presence of the contact reaction of the ground.

6. Conclusions

In this paper, we presented an efficient methodology that can be applied to control the progressive collapse of 2D reinforced-concrete frame structures.

First, we described the stress-resultant Timoshenko finite element with embedded discontinuity in rotation. Such model based on elasto-plastic law with bilinear isotropic hardening followed by softening. The concept of softening plastic hinge is modeled to capture the post-peak softening behavior. The cantilever beam and two-story frames illustrate that the presented model is able to describe the response of reinforced-concrete frame up to complete failure and mechanism creation.

Second, we showed here nonlinear dynamic analysis can be performed with the mechanism created in first phase. The complete collapse computations also consider the contact between the building and the ground using penalty method, to investigate the progressive collapse of the frame structures up to total collapse. The presented six-story reinforced-concrete 2D frame illustrates that the strategy proposed in this paper is capable to describe the progressive collapse process for reinforced concrete 2D frame structures. The final failure mechanism depends upon the softening modulus, triggering small or large number of plastic hinges.

An efficient conserving/decaying energy scheme is used for solving dynamic governing equations. The scheme introduces a desirable numerical dissipation of high frequency oscillations that can be observed in dynamic structure response, especially when triggering the contact of the

structure with ground.

The numerical examples illustrate the efficiency of the methodology proposed and its ability to describe the controlled progressive collapse of 2D reinforced-concrete frame structures in rather realistic way. The results are direct interest for controlled destruction in densely constructed urban areas.

References

Armero F. and Ehrlich D. (2006), "Numerical modeling of softening hinges in thin Euler-Bernoulli beams", *Comput*. *Struct*., **84**, 641-656.

Brank, B., Briseghella, L., Tonello, N. and Damjanic, F. (1998), "On non-linear dynamics of shells: Implementation of energy-momentum conserving algorithm for a finite rotation shell model", *J*. *Numer*. *Meth*. *Eng*., **42**, 409-442.

Bui, N.N., Ngo, M., Nikolic, M., Brancherie, D. and Ibrahimbegovic, A. (2014), "Enriched Timoshenko beam finite element for modeling bending and shear failure of reinforced concrete frames", *Comput*. *Struct*., **143**, 9-18.

Dujc, J., Brank, B. and Ibrahimbegovic, A. (2010), "Multi-scale computational model for failure analysis of metal frames that includes softening and local buckling", *Comput*. *Meth*. *Appl*. *Mesh*. *Energy*, **199**, 1371-1385.

Hartmann, D., Breidt, M., Nguyen, V.V., Stangenberg, F., Höhler, S., Schweizerhof, K., Mattern, S., Blankenhorn, G., Möller, B. and Liebscher, M. (2008), *On a Fundamental Concept of Structural Collapse Simulation Taking into Account Uncertainty Phenomena*, In: A. Ibrahimbegovic, M. Zlatar (eds.) *Damage Assessment and Reconstruction after War or Natural Disasters*, Springer, The Netherlands, NATO Science for Peace and Security Series C, Environmental Security (2009).

Humberto Breves, C. and Rodrigo Ribeiro, P. (2014), "A total lagrangian position-based FEM applied to physical and geometrical nonlinear dynamics of plane frames including semi-rigid connections and progressive collapse", *Fin*. *Elem*. *Analy*. *Des*., **91**, 1-15.

Ibrahimbegovic, A. (2009), *Non-Linear Solid Mechanics*, Springer.

Ibrahimbegovic, A. and Frey, F. (1993a), "Finite element analysis of linear and nonlinear planar deformation of elastic initially curved beams", *J*. *Numer*. *Meth*. *Eng*., **36**, 3239-3258.

Ibrahimbegovic, A. and Frey, F. (1993b), "Stress resultant finite element analysis of reinforced concrete plates", *J*. *Eng*. *Comput*., **10**, 15-30.

Ibrahimbegovic, A. and Mamouri, S. (1999), "Nonlinear dynamics of flexible beams in planar motion: formulation and time-stepping scheme for stiff problems", *Comput*. *Struct*., **70**, 1-22.

Ibrahimbegovic, A. and Mamouri, S. (2000), "On rigid components joint constraints in nonlinear dynamics of multibody systems employing 3D geometrically exact beam model", *Comput*. *Meth*. *Appl*. *Mesh*. *Energy*, **188**, 805-831.

Ibrahimbegovic, A. and Mamouri, S. (2002), "Energy conserving decaying implicit time stepping scheme for nonlinear dynamics of three dimensional beams undergoing finite rotations", *Comput*. *Meth*. *Appl*. *Mesh*. *Energy*, **191**, 4241-4258.

Imamovic, I., Ibrahimbegovic, A. and Mesic, E. (2017), "Nonlinear kinematics Reissner's beam with combined hardening/softening elastoplasticity", *Comput*. *Struct*., **189**, 12-20.

Imamovic, I., Ibrahimbegovic, A., Knopf-Lenoir, C. and Mesic, E. (2015), "Plasticity-damage model parameters identification for structural connections", *Coupled Syst*. *Mech*., **4**, 337-364.

Juarez, G. and Ayala, A.G. (2012), "Finite element variational formulation for beams with discontinuities", *Fin*. *Elem*. *Analy*. *Des*., **54**, 37-47.

Jukic, M., Brank, B. and Ibrahimbegovic, A. (2013), "Embedded discontinuity finite element formulation for failure analysis of planar reinforced concrete beams and frames", *Eng*. *Struct*., **50**, 115-125.

Jukic, M., Brank, B. and Ibrahimbegovic, A. (2014), "Failure analysis of reinforced concrete frames by

beam finite element that combines damage, plasticity and embedded discontinuity", *Eng. Struct.*, **75**, 507-527.

Mamouri, S., Hammadi, F. and Ibrahimbegovic, A. (2014), "Decaying\conserving implicit scheme and nonlinear instability analysis of 2D frame structures", *J. Non-lin. Mech.*, **67**, 144-152.

Mamouri, S., Kouli, R., Benzegaou, A. and Ibrahimbegovic, A. (2016a), "Implicit controllable high-frequency dissipative scheme for nonlinear dynamics of 2D geometrically exact beam", *Nonlin. Dyn.*, **84**(3), 1289-1302.

Mamouri, S., Mourid, E. and Ibrahimbegovic, A. (2016b), "Study of geometric non-linear instability of 2D frame structures", *Eur. J. Comput. Mech.*, **24**(6), 256-278.

Michaloudis, G., Blankenhorn, G., Mattern, S. and Schweizerhof, K. (2010), *Modelling Structural Failure with Finite Element Analysis of Controlled Demolition of Buildings by Explosives Using LS-DYNA*, In: Nagel, W., Kröner, D. and Resch, M. (eds), High Performance Computing in Science and Engineering '09. Springer, Berlin, Heidelberg.

Michaloudis, G., Mattern, S. and Schweizerhof, K. (2011), *Computer Simulation for Building Implosion Using LS-DYNA*, In: Nagel, W., Kröner, D. and Resch, M. (eds), High Performance Computing in Science and Engineering '10. Springer, Berlin, Heidelberg.

Nanakorn, P. (2004), "A two-dimensional beam–column finite element with embedded rotational discontinuities", *Comput. Struct.*, **82**, 753-762.

Ngo, V.M., Ibrahimbegovic, A. and Brancherie, D. (2014), "Stress-resultant model and finite element analysis of reinforced concrete frames under combined mechanical and thermal loads", *Coupled Syst. Mech.*, **3**, 111-144.

Pham, B.H., Brancherie, D., Davenne, L. and Ibrahimbegovic, A. (2013), "Stress-resultant models for ultimate load design of reinforced concrete frames and multi-scale parameter estimates", *Comput. Mech.*, **51**, 347-360.

Piculin, S. and Brank, B. (2015), "Weak coupling of shell and beam computatinal models for failure analysis of steel frames", *Fin. Elem. Analy. Des.*, **97**, 20-42.

Rodolfo André, K. and Humberto Breves, C. (2017), "Flexible multibody dynamics finite element formulation applied to structural progressive collapse analysis", *Lat. Am. J. Sol. Struct.*, **14**, 52-71.

Wu, J.Y. (2013), "New enriched finite elements with softening plastic hinges for the modeling of localized failure in beams", *Comput. Struct.*, **128**, 203-218.

Zienkiewicz, O.C. and Taylor, R.L. (2005), *The Finite Element Method*, Vol. I, II, III.

AI